

# Polarimetric Modelling of Ocean Backscatter and Brightness Temperatures

Simon H. Yueh

Jet Propulsion Laboratory, MS 300-235  
California Institute of Technology  
4800 Oak Grove Drive, Pasadena, CA 91109, USA  
Tel: 818-354-3012, Fax: 818-393-5285  
E-mail: [simon@stokes2.jpl.nasa.gov](mailto:simon@stokes2.jpl.nasa.gov)

Abstract ‘There has been an increasing interest in the applications of polarimetric microwave radiometers for ocean wind remote sensing. Aircraft and spaceborne radiometers have found a few Kelvins wind direction signals in sea surface brightness temperatures, in addition to their sensitivities on wind speeds. However, it was not clear what physical scattering mechanisms produced the observed brightness dependence on wind direction. To this end, polarimetric microwave emissions from wind-generated sea surfaces are investigated with a polarimetric two-scale scattering model, which relates the directional wind-wave spectrum to passive microwave signatures of sea surfaces. Theoretical azimuthal modulations are found to agree well with the Jet Propulsion Laboratory (JPL) Wind Radiometer (WINDRAD) observations of all Stokes parameters for a large range of wind speeds. This theoretical interpretation suggests the use of polarimetric brightness temperatures for retrieving the directional wave spectrum of short gravity and capillary waves. The polarimetric backscattering coefficients of sea surfaces are also explored using this scattering model with results in reasonable agreement with airborne and satellite scatterometer measurements and the symmetric relations expected for reflection-symmetric surfaces.

## I. INTRODUCTION

‘There has been an increasing interest in the application of polarimetric microwave radiometers for ocean wind velocity (speed and direction) measurements. Early experimental results, such as those published in [1, 2], have shown the correlation of sea surface brightness temperatures with the near surface wind speed. Theoretical investigations by [3, 4] have determined that a two-scale scattering model could interpret reasonably well the wind speed sensitivity of vertically and horizontally polarized brightness temperatures ( $T_v$  and  $T_h$ ). In addition to wind speed sensitivity, microwave sea surface radiation has been shown by recent aircraft and spacecraft radiometer observations to have a few Kelvin directional signals [5, 6, 7, 8, 9]. A re-examination of theoretical scattering models is therefore required to shed light on the physics behind the observed wind direction signatures.

Ocean wind roughens surfaces in the form of gravity and capillary waves, breaking waves and foam. The scattering effects of large-scale waves have been modeled by the geometric optics (GO) scattering theory [10, 11]. In GO

models, the large-scale waves are modeled by tilting surface facets, and the scattering coefficients are proportional to the number of surface facets with a tilting angle satisfying the specular reflection condition. Stogryn [10] used Cox and Munk’s slope distribution of sea surfaces [12] and studied the sensitivity of brightness temperatures to wind speed. However, Hollinger’s tower measurements [1] performed at 1, 8 and 19 GHz showed that the GO model failed to account for the observational frequency dependence and significantly underestimated the wind speed dependence of the horizontally polarized radiation at small incidence angles. With the Bragg scattering mechanism taken into consideration, the two-scale scattering theory [13] was extended by Wu and Fung [3] and Wentz [4] to interpret the brightness temperatures of sea surfaces. In the two-scale scattering model, the Bragg scattering by small-scale waves contributes to bistatic incoherent scattering and modifies the coherent reflection coefficients of large-scale waves. As compared with the geometric optics model, the two-scale theory more accurately modeled the dependence of brightness temperatures on incidence angles and wind velocities [3, 4].

However, the contributions of short and long waves to the wind direction signals in passive microwave radiometer measurements [5, 6, 7, 8, 9] have not yet been thoroughly investigated. In Wu and Fung’s [3] and Wentz’s [4] models, the surface spectrum of short waves was assumed to be isotropic and the Bragg scattering theory for isotropic surfaces was used. Consequently, no directional dependence was predicted by their theoretical models. In contrast, Stogryn’s GO model using Cox and Munk’s slope distribution, although in poor agreement with the wind speed sensitivity of sea surface brightness temperatures, did predict an azimuthal brightness variation of a few Kelvins. The effects of Bragg scattering by anisotropic short-gravity and capillary waves on all Stokes parameters [15] were not studied until recently [16] and the theoretical results appeared to agree with the measurements made at near normal incidence angles [6]. Additionally, Irisov et al. [17] evaluated the difference between upwind and crosswind observations of brightness temperatures using a two-scale model based on the theory of critical phenomena and Cox and Munk’s slope distribution, and they showed that the contribution from capillary waves was much more significant than that from long waves at the frequencies of 19 and 37 GHz at normal incidence angle and that taking into account all scattering mechanisms was necessary at

the incidence angle of  $78^\circ$ . However, Isov et al.'s analysis was limited to the upwind and crosswind asymmetry of  $T_v$  and  $T_h$  with no results simulated for the other Stokes parameters, and they did not provide predictions for the range of incidence angles from  $30^\circ$  to  $70^\circ$ , where significant changes of upwind and downwind asymmetry were observed in [7, 8, 9].

The purpose of this paper is to examine the applicability of a two-scale model [18, 19] to the wind direction signals in polarimetric sea surface brightness temperatures. This model was a generalization of Durden and Vesecky's scattering model [20] to polarimetric microwave emission, extending the previous two-scale models [3, 4] to surfaces with an anisotropic directional spectrum and providing theoretical predictions for all four Stokes parameters of sea surface brightness temperatures. This allows us to examine the relative significance of geometric tilting effects of long waves, Bragg scattering by short waves, the excess emission from sea foam and the modulation of short waves by long waves (hydrodynamic modulation) [20, 21, 22, 23, 24].

In Section I, the theory of polarimetric radiometry is summarized. Section III. presents a two-scale model for thermal emission from anisotropic wind waves and foam. Section IV. presents comparison of theoretical results and existing microwave brightness temperatures of sea surfaces. Section V. summarizes the results of this paper and discusses the issues for further investigation.

## II. POLARIMETRIC RADIOMETRY

The electromagnetic waves emitted from natural media due to random thermal motion of electric charges are in general partially polarized. To fully characterize the polarization state of partially polarized thermal radiation, four parameters  $I, Q, U,$  and  $V$  were introduced by Sir George Stokes. Because conventional radiometers for earth remote sensing perform  $T_v$  and  $T_h$  measurements, an alternate representation of the Stokes vector uses four parameters,  $T_v, T_h, U,$  and  $V,$

$$I_s = \begin{bmatrix} T_v \\ T_h \\ U \\ V \end{bmatrix} = c \begin{bmatrix} \langle |E_v|^2 \rangle \\ \langle |E_h|^2 \rangle \\ 2\text{Re} \langle E_v E_h^* \rangle \\ 2\text{Im} \langle E_v E_h^* \rangle \end{bmatrix} \quad (1)$$

$T_v$  and  $T_h$  are the brightness temperatures of vertical and horizontal polarizations, while  $U$  and  $V$  characterize the correlation between these two orthogonal polarizations. Note that  $I (=T_v + T_h)$  represents the total radiated energy and  $Q (=T_v - T_h)$  the polarization balance. Eq. (1) defines the Stokes parameters in terms of the horizontally and vertically polarized components of electric fields ( $E_h$  and  $E_v$ ). The polarization vectors are related to the direction of propagation and are defined in [16]. The angular brackets denote the ensemble average of the argument, and  $c$  is a constant relating the brightness temperature to the electric energy density [15, 25].

Recent interests in the applications of polarimetric radiometry for remote sensing were motivated by the theoretical work [15, 26]. Ground-based experiments were

carried out to investigate the Stokes parameters of thermal emission from periodic soil surfaces at X-band [27] and from sinusoidal water surfaces at Ku band [28], at X band [29], and at 94-GHz [11]. The surface profiles studied in these experiments were one-dimensional with an rms height of a few centimeters, much rougher than the capillary waves in the open oceans. Hence, the measured brightness temperatures had an azimuthal variation of as large as 20 Kelvins, significantly larger than the measurements from ocean surfaces [5, 7, 8] and the theoretical predictions [18, 30]. However, these studies clearly show that the Stokes parameters of microwave radiation from surfaces with preferential directional features are functions of azimuthal viewing angles.

For wind-generated sea surfaces, the surface spectrum is symmetric with respect to the wind direction ( $\phi_w$ ) or the surfaces are statistically reflection symmetric with respect to  $\phi_w$  [31], if the effects of swell can be ignored. Denoting the azimuthal observation angle of radiometer look direction by  $\phi_r$  and the relative azimuth angle by  $\phi = \phi_w - \phi_r$ , Yueh et al. [31] derived from Maxwell's equations that  $T_v$  and  $T_h$  are even functions of  $\phi$  and that  $U$  and  $V$  are odd functions for reflection-symmetric surfaces.

The even and odd symmetry properties allow us to expand the Stokes parameters in either cosine or sine series of the azimuth angle  $\phi$ . Hence, expanded to the second harmonic of  $\phi$ ,

$$T_v \simeq T_{v0} + T_{v1} \cos \phi + T_{v2} \cos 2\phi \quad (2)$$

$$T_h \simeq T_{h0} + T_{h1} \cos \phi + T_{h2} \cos 2\phi \quad (3)$$

$$U \simeq U_1 \sin \phi + U_2 \sin 2\phi \quad (4)$$

$$V \simeq V_1 \sin \phi + V_2 \sin 2\phi \quad (5)$$

The first harmonics account for the upwind and downwind asymmetric surface features, while the second harmonics for the upwind and crosswind asymmetry. The coefficients of these Fourier series are functions of oceanic, atmospheric, and some instrument parameters, including near surface wind velocity, swell, salinity, air and sea surface temperatures, incidence angle, polarization and frequency. The dominant geophysical parameter is the surface wind velocity according to the past experience of ocean backscatter measurements. However, other variables which may influence the wind stress or friction velocity, could become significant at low to moderate wind speeds. Understanding the relation of these harmonic coefficients with geophysical parameters is crucial to the inversion of geophysical parameters using polarimetric brightness temperatures.

### 111. POLARIMETRIC 2-SCALE SEA SURFACE EMISSION MODEL

Two-scale sea surface models approximate the sea surface as a two-scale surface with small-scale ripples or capillary waves riding on the top of large-scale surfaces. With this approximation, the total thermal emission from the surface is the sum of emissions from individual, slightly perturbed surface patches tilted by the underlying large-scale surface. Although two-scale models have demonstrated reasonable numerical accuracy [3, 4, 17, 20, 22],

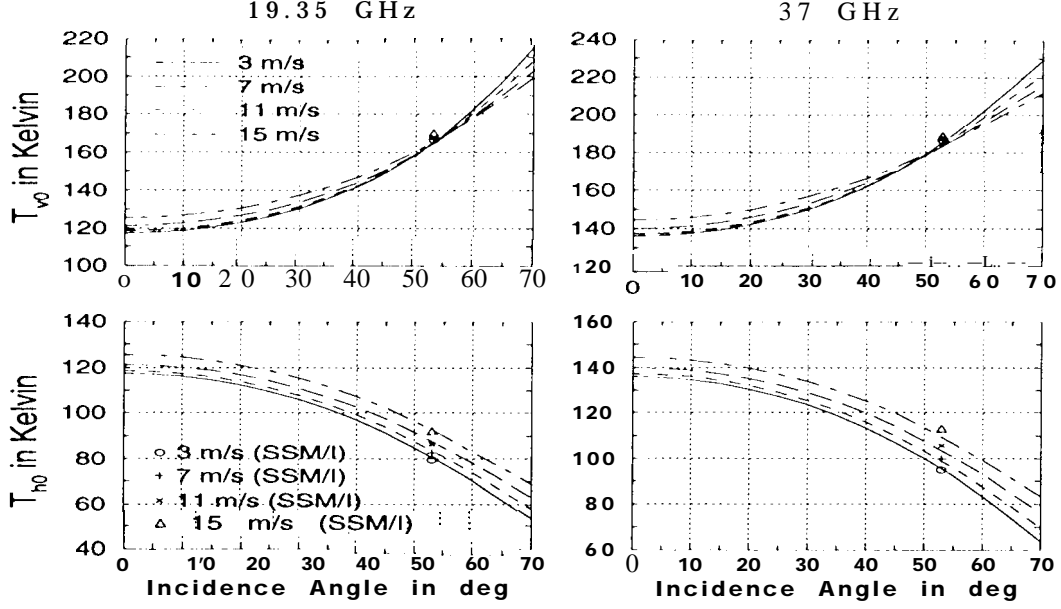


Figure 1.  $T_{v0}$  and  $T_{h0}$  as functions of incidence angles for several wind speeds calculated from the two-scale model at 19.35 and 37 GHz frequencies.  $T_{v0}$  and  $T_{h0}$  from Wentz's SSM/I geophysical model function [7] are included for comparison.  $T_s = 12^\circ \text{C}$ .

the two-scale theory remains an approximate numerical model for ocean surface scattering and emission. The accuracy of two-scale models relies on the accuracies of two modelling components: the sea surface model and electromagnetic scattering theories. A typical mathematical representation of gravity and capillary waves is the sea surface spectrum, which remains an important area for research [32], particularly the wavenumber spectrum of capillary waves. Furthermore, mathematical models of breaking waves and foam were not yet adequate for fully polarimetric scattering modelling. The electromagnetic modelling portion of two-scale models was also heuristic in many areas. Hence, though it is shown in the following sections that the two-scale model appears to provide reasonable comparison with experimental data, more rigorous theories will definitely benefit the study of air-sea interaction processes using polarimetric radiometer data.

In the two-scale model, the Stokes vector of the thermal emission from a local surface patch is represented by  $I_{sl}$ . 10 account for the radiation from sea foam,  $I_{sl}$  is written as the sum of two terms, including the Stokes vector of the emission from foam-free, wind-roughened small-scale sea surfaces and that from the surface patches with 100 percent foam coverage, denoted by  $I_{ss}$  and  $I_{sf}$ , respectively. Hence,

$$I_{sl} = (1 - F_r)I_{ss} + F_r I_{sf} \quad (6)$$

with  $F_r$  representing the areal percentage coverage of sea foam over sea surfaces.  $F_r$  is known to be a function of surface wind velocities as well as air and sea surface

temperatures, and is calculated using the empirical sea foam fractional coverage algorithm [33], a least square fit of experimental observations.

The Stokes vector of the two-scale surface is written as the average of  $I_{sl}$  over the slope distribution of large scale surfaces, denoted by  $P(S_x, S_y)$ . In addition to changing the local incidence and azimuth angles, the tilting angles of large scale surfaces affect the area of surface patch projected along the line of sight, meaning that the emission from small scale surfaces has to be further weighted by the solid angle of the large-scale surface viewed by the radiometer [34, 35]. This results in the weighting factor  $(1 - S_x \tan \theta)$  for the Stokes vector observed at the incidence angle  $\theta$  and azimuth angle  $\phi$ , and the derivation of the following equation is similar to that shown in [34].

$$I_s = \int_{-\infty}^{\infty} dS'_y \int_{-\infty}^{\cot \theta} dS'_x I_{sl} (1 - S'_x \tan \theta) P(S_x, S_y) \quad (7)$$

where

$$\begin{aligned} S_x &= S'_x \cos \phi - S'_y \sin \phi \\ S_y &= S'_x \sin \phi + S'_y \cos \phi \end{aligned} \quad (8)$$

In the above equations,  $S_x$  and  $S_y$  represent the surface slopes in  $x$  (upwind) and  $y$  (crosswind) directions, while  $S'_x$  and  $S'_y$  represent the surface slopes along and across the radiometer azimuth observation direction, respectively. Integration over  $S'_x$  has to be limited to  $\cot \theta$  to account for the shadowing by large-scale surfaces.

For the results presented in this paper, the integral for  $I_s$  was carried out numerically with the integration limits of  $S_x$  and  $S_y$  truncated at 5 times of the rms upwind and crosswind slopes ( $S_u$  and  $SC$ ), respectively, which were calculated from Eqs. (11) and (12). The integrand  $I_{sl}$  required the numerical calculations of  $I_{ss}$  and  $I_{sf}$ .  $I_{ss}$  involved two double integrals, while  $I_{sf}$  was calculated with an empirical formula [37] and did not require numerical integration. Hence, the numerical results for  $I_s$  were obtained from the numerical integration of a quadruple integral.

In the following subsections, we describe the empirical surface spectrum used for the two-scale model and the formulas used to calculate the Stokes vectors of foam-free, small-scale sea surfaces and sea foam.

#### A. Sea surface model

In two-scale models, the surface spectra of large-scale waves and small-scale waves, denoted by  $W_l$  and  $W_s$ , respectively, are related to the sea surface spectrum  $W$  by

$$W_l(K, \phi_k) = \begin{cases} W(K, \phi_k) & \text{if } K < k_d \\ 0 & \text{otherwise} \end{cases} \quad (9)$$

$$W_s(K, \phi_k) = \begin{cases} 0 & \text{if } K < k_d \\ W(K, \phi_k) & \text{otherwise} \end{cases} \quad (10)$$

where  $k_d$  is the two-scale cutoff. The slope distribution function  $P(S_x, S_y)$  of large-scale waves is assumed to be zero-mean Gaussian with the upwind and crosswind slope **variances**,  $S_u^2$  and  $S_c^2$ , which are calculated from all surface spectral components with a wavenumber less than  $k_d$ ,

$$S_u^2 = \int_0^\infty dK \int_0^{2\pi} d\phi_k K^3 \cos^2 \phi_k W_l(K, \phi_k) \quad (11)$$

$$S_c^2 = \int_0^\infty dK \int_0^{2\pi} d\phi_k K^3 \sin^2 \phi_k W_l(K, \phi_k) \quad (12)$$

$S_u$  and  $SC$  are the rms upwind and crosswind surface slopes.

It is known that the hydrodynamic modulation makes the short waves more concentrated on the leeward faces of large-scale waves [21]. This phenomenon is evident in Fig. 6 of the paper [22], and has been employed to interpret the difference between upwind and downwind sea surface backscattering cross sections [20, 22, 23, 24]. The hydrodynamic modulation was typically modelled by modulating the spectrum of small-scale waves with a parameter  $h$  based on the slope of large-scale waves [20, 22, 24].

$$W_s(K, \phi_k, s) = h W_s(K, \phi_k) \quad (13)$$

Specifically, the parameter  $h$  was assumed to take the following form in this paper:

$$h = \begin{cases} 1 - 0.5 \operatorname{sgn}(S_x) & \text{if } |S_x/S_u| > 1.25 \\ 1 - 0.4 S_x/S_u & \text{if } |S_x/S_u| \leq 1.25 \end{cases} \quad (14)$$

where  $\operatorname{sgn}(S_x) = 1$  if  $S_x$  is positive and  $\operatorname{sgn}(S_x) = -1$  if  $S_x$  is negative. Consequently, the ripples on the leeward faces of long waves are enhanced and those on the

windward side are depressed. This functional form is consistent with the description of hydrodynamic modulation by Reece [21] and is similar to the modulation models assumed in [20, 22, 24] for sea surface backscatter. The magnitude of modulation  $h$  is larger than that assumed in [20], but smaller than that assumed in [24]. Note that it might appear that this modulation model is stronger than that shown in Eq. (20) in [22]. However, the surface spectrum model assumed in [22] had an additional modulation term described by Eq. (12) in [22], which produced an extra upwind and downwind asymmetry in the wavenumber spectrum. Hence, the magnitude of  $h$  appeared to be consistent with the modulation models assumed in previous ocean backscattering models.

#### B. Emission from Small-scale Waves

To extend two-scale models [3, 4] to anisotropic sea surfaces, the second-order perturbation solution of Bragg scattering from small-scale, anisotropic surfaces [16] is used to calculate  $I_{ss}$ . The energy conservation condition, crucial for calculating the brightness temperature using the Kirchhoff's law [36], was verified with the numerical Monte Carlo simulations of rough surface scattering [16].

The Stokes emission vector  $I_{ss}$  in the earth coordinate is related to that denoted by  $I'_{ss}$  in the local surface coordinate by the coordinate rotation shown in Appendix A. By using a polarimetric Kirchhoff's law [25, 26],  $I'_{ss}$  is related to the reflectivity vector  $(1, \cdot)$  of the small-scale sea surface by

$$I'_{ss} = T_s \begin{pmatrix} 1 \\ 1 \\ 0 \\ 0 \end{pmatrix} - I_r \quad (15)$$

where  $T_s$  is the surface temperature.

Based on the second order solution of scattering from slightly perturbed rough surfaces [16],  $I_r$  is the sum of two terms,  $I_{rc}$  and  $I_{ri}$ :

$$I_r = I_{rc} + I_{ri} \quad (16)$$

$I_{ri}$  represents the incoherent surface reflectivity, and is calculated by integrating incoherent polarimetric bistatic scattering coefficients  $\gamma_{\alpha\beta\mu\nu}^i(\theta_l, \phi_l; \theta_i, \phi_i)$  over all incidence angles in the upper hemisphere. The coherent reflectivity  $I_{rc}$  accounts for the specular reflectivity with corrections by the second order scattered fields. The detailed expressions of  $I_{ri}$  and  $I_{rc}$  are given in [16].

#### C. Emission from foam

Although foam typically covers only a few percent of sea surfaces, increasing foam coverage on the sea surface can substantially increase the sea surface emissivity [37, 38]. Previous theoretical foam scattering models, although having offered physical insight into the excess brightness temperature contribution by sea foam, are not yet accurate enough to predict the polarization properties and incidence angle dependence of microwave emission from foam. Further research on the polarization signatures of foam is imperative.

Due to the lack of a rigorous theoretical scattering model for foam, Stogryn's empirical emissivity model of

## 19 GHz DATA AND MODEL AT 55° INCIDENCE

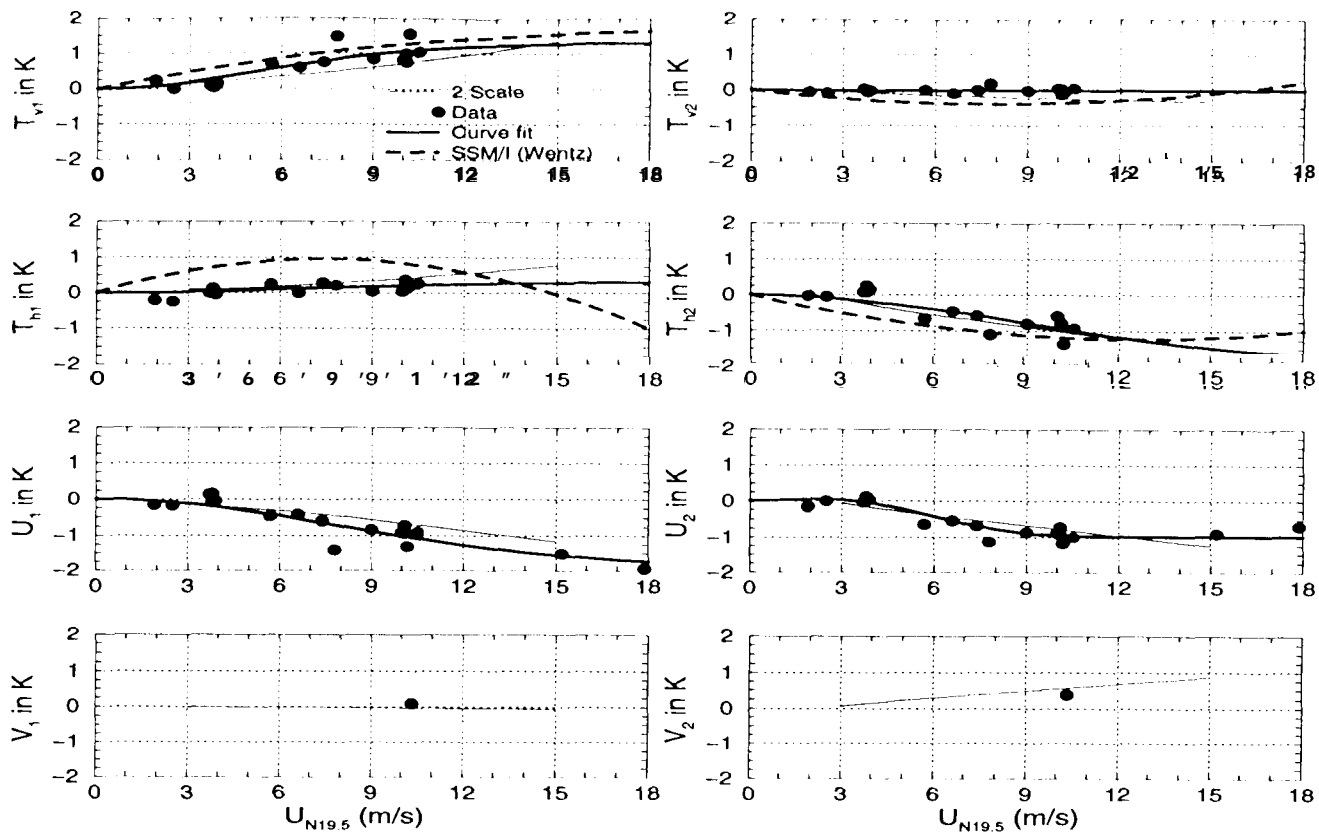


Figure 2. Comparison of measured first and second harmonic coefficients with 2-scale model predictions at 19,35 GHz and 55° incidence angle.  $k_d = 150$  1/m and  $T_s = 12^\circ$  C. Model values from Wentz’s SSM/I geophysical model function [7] are included for comparison.  $T_s = 12^\circ$  C.

sea foam [37] is used to calculate the emissivities of vertical and horizontal polarizations in the local surface coordinate. The Stokes vector in the local surface coordinate is then transformed to  $I_{sf}$  in the earth surface coordinate using the coordinate transformation described in Appendix A.

### IV. COMPARISON WITH EXPERIMENTAL DATA

In this section, the wind direction signals in microwave brightness temperatures of sea surfaces acquired by the JPL aircraft WINDRAD flights over a large range of wind speeds [8, 9, 45] are interpreted using the two-scale model described in the previous section.

Model inputs required for theoretical calculations include the surface spectrum  $W$  and the sea surface permittivity. The empirical surface spectrum  $W$  proposed by Durden and Vesecky [20] was used for model calculation. (Because some typographical errors are found in their paper, the correct expressions of Durden and Vesecky’s spectrum can be found in Appendix B.) Klein and Swift’s dielectric model [39] is used to calculate the sea surface dielectric constant with an assumed water salinity of 35 parts per thousand and surface temperatures measured by buoys.

Figure 1 illustrates theoretical  $T_{v0}$  and  $T_{h0}$  versus incidence angles for four wind speeds: 3, 7, 11, and 15  $\text{m}\cdot\text{s}^{-1}$ . The sea surface temperature of  $12^\circ\text{C}$  was assumed for theoretical calculations. Wentz’s SSM/I geophysical model function [7] was evaluated at the same wind speeds and the same sea surface temperature. There were some differences between the absolute values of theoretical and SSM/I model predictions. It had been pointed out in [7, 40] that Klein and Swift’s dielectric model [39], which was constructed with data acquired at less than 10 GHz, needed to be adjusted if applied to frequencies above 10 GHz. Since Wentz [7, 40] had tuned Klein and Swift’s dielectric model to obtain the SSM/I model, part of the difference between Wentz’s SSM/I model and the two-scale model simulations could be attributed to the difference of dielectric models. The other cause of difference is the model for sea foam emission. While Stogryn’s sea foam emission model [37] used in the two-scale model was expected to be reasonable, it should not be expected to be in absolute agreement with the SSM/I observations. However, the difference was not expected to have a significant impact on the wind speed sensitivities of theoretical  $T_{v0}$  and  $T_{h0}$ , and it was shown in Figure 1 that there was a reasonable agreement between the two-scale theory and Wentz’s SSM/I geophysical model for the wind speed

### 37 GHz DATA AND MODEL AT 55° INCIDENCE

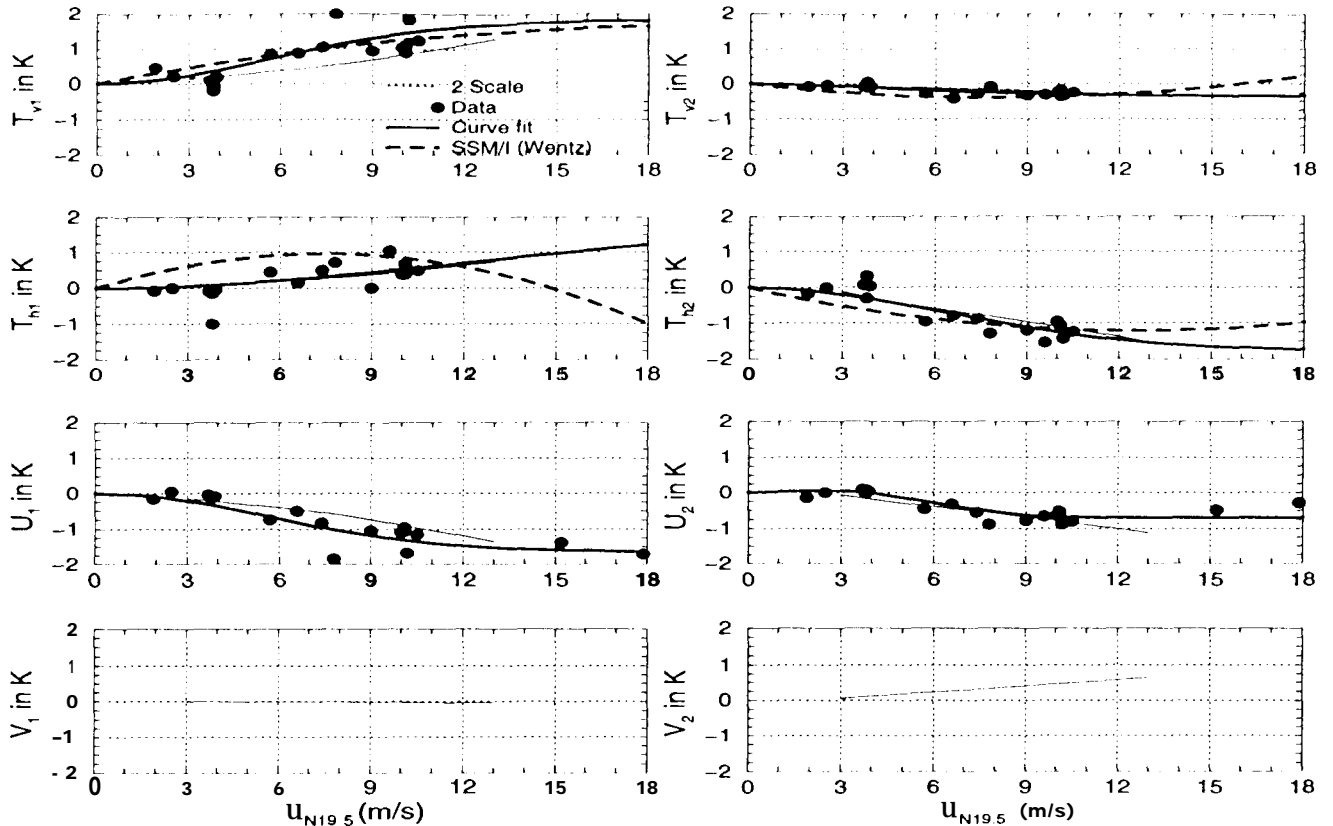


Figure 3. Comparison of measured first and second harmonic coefficients with 2-scale model predictions at 37 GHz and 55° incidence angle,  $k_d = 150 \text{ 1/m}$  and  $T_s = 12^\circ \text{ C}$ . Wentz's SSM/I model values at 53° incidence angle are included for comparison.

sensitivities of  $T_{v0}$  and  $T_{h0}$ . Theoretical wind speed sensitivities of  $T_{v0}$  are positive at low incidence angles and negative at incidence angles larger than 60°, just like the experimental data reported in [1, 2] and the theoretical results [4]. Theoretical 19 GHz  $T_{v0}$  has no wind speed sensitivity at about 55°, while the zero wind speed sensitivity for theoretical 37 GHz  $T_{v0}$  occurs at a smaller incidence angle of about 50°. This is because the dielectric constant of sea surfaces at 37 GHz is smaller than that at 19 GHz. A smaller dielectric constant leads to a smaller Brewster angle for 37 GHz and consequently, a smaller incidence angle where the wind speed sensitivity of  $T_{v0}$  makes a transition from positive to negative numbers. Note that although the wind speed sensitivity of  $T_{v0}$  in Wentz's SSM/I geophysical model is small, it remains positive at 37 GHz and is inconsistent with the small negative sensitivity from the model at 53° incidence angle. However, Hollinger's 19 GHz data [1] showed that there is no wind speed sensitivity at about 60° incidence angles, while the  $T_v$  data from Sasaki et al. [2] showed a zero crossing at about 55°. This suggests that the wind speed sensitivities of  $T_{v0}$  in the range of incidence angles from 50° to 60° could be sensitive to other surface parameters, for example, the sea surface dielectric constant as well as the areal coverage and brightness properties of sea foam. Further refinements of these model inputs could be neces-

sary to achieve a better accuracy for  $T_{v0}$  between 50° and 60° incidence angles. Unlike the vertical polarization,  $T_{h0}$  increases with increasing wind speeds at all incidence angles, and theoretical  $T_{h0}$  has a slightly larger wind speed sensitivity at higher incidence angles. This agrees with the experimental observations of the wind speed sensitivity of  $T_{h0}$  [1, 2].

Figures 2 and 3 plot the first and second harmonic coefficients of all Stokes parameters acquired from the JPL WINDRAD flights from 1994 to 1996 [45] as a function of wind speed at 55° incidence angle. To avoid the effects of clouds, we only include the WINDRAD data acquired from flights with clear skies and thin clouds. It can be seen that the theoretical harmonic coefficients agree reasonably well with the JPL WINDRAD data acquired from 1994 to 1996 over a large range of wind speeds. This suggests that the scattering mechanisms dominating the directional signatures of sea surface brightness temperatures have been considered in the two-scale scattering model. A sensitivity study has been conducted and shows that the dominant scattering mechanism is the Bragg scattering by short-gravity and capillary waves.

In Figures 2 and 3, both data and theory show that the direction signal in  $T_v$  is dominated by the first harmonic, while that of  $T_h$  is dominated by the second harmonic at near 55° incidence angle. The combined effects of hydro-

dynamic modulation and Brewster angle [44] have been employed to explain these signatures.

Figures 2 and 3 also include Wentz's SSM/ $T_v$  and  $T_h$  model coefficients at  $53^\circ$  incidence angle [7] for comparison with the theory and JPL WINDRAD data. There is a reasonable agreement for  $T_{v1}$ ,  $T_{v2}$ , and  $T_{h2}$ . However, the direction signals predicted by Wentz's SSM/I model remain quite significant at low wind speeds ( $<5$  m/s) while WINDRAD data and theory show a much weaker signal. In addition,  $T_{h1}$  from Wentz's SSM/I model is very different from the WINDRAD data and theoretical predictions. It is not yet clear what causes these discrepancies.

As an independent check of the theoretical model, a polarimetric two-scale scattering model was constructed based on the approach described in previous section with the Stokes emission vector replaced by polarimetric backscattering coefficients [43]. In addition, the theoretical model can also provide estimates of polarimetric backscattering coefficients of sea surfaces, which have not yet been collected at frequencies above 10 GHz.

As noted in [31], the conventional backscattering coefficients  $\sigma_{hh}$ ,  $\sigma_{vv}$ ,  $\sigma_{hv}$ , and  $\sigma_{vh}$  and the correlations between two co-polarized or two cross-polarized responses are even functions of  $\phi$ :

$$\sigma_{hh}(\theta, -\phi) = \sigma_{hh}(\theta, \phi) \quad (17)$$

$$\sigma_{vv}(\theta, -\phi) = \sigma_{vv}(\theta, \phi) \quad (18)$$

$$\sigma_{hhvv}(\theta, -\phi) = \sigma_{hhvv}(\theta, \phi) \quad (19)$$

$$\sigma_{hv}(\theta, -\phi) = \sigma_{hv}(\theta, \phi) \quad (20)$$

$$\sigma_{vh}(\theta, -\phi) = \sigma_{vh}(\theta, \phi) \quad (21)$$

$$\sigma_{hvvh}(\theta, -\phi) = \sigma_{hvvh}(\theta, \phi) \quad (22)$$

while the correlations between co- and cross-polarized backscatters are odd functions:

$$\sigma_{hhhv}(\theta, -\phi) = -\sigma_{hhhv}(\theta, \phi) \quad (23)$$

$$\sigma_{hhvh}(\theta, -\phi) = -\sigma_{hhvh}(\theta, \phi) \quad (24)$$

$$\sigma_{hvvv}(\theta, -\phi) = -\sigma_{hvvv}(\theta, \phi) \quad (25)$$

$$\sigma_{vhvv}(\theta, -\phi) = -\sigma_{vhvv}(\theta, \phi) \quad (26)$$

where  $\theta$  and  $\phi$  represent the incidence and azimuth angles of the radar observation directions. The above equations show that the backscattering coefficients  $\sigma_{hh}$  and  $\sigma_{vv}$  are even functions of the azimuth angle  $\phi$ . This has been well known in the microwave backscattering coefficients of wind-generated sea surfaces, which are symmetric with respect to the wind direction. For example, the SASS geophysical model function [Wentz et al., 1984], empirically relating the ocean wind vectors to the microwave backscattering coefficient  $\sigma_0$  ( $\sigma_{hh}$  or  $\sigma_{vv}$ ) by a cosine series, which is an even function of the azimuth angle  $\phi$ . Figures 4(a) and (b) illustrates  $\sigma_{vv}$  and  $\sigma_{hh}$ , calculated using the SASS geophysical model function, as a function of  $\phi$  for the wind speed of 11.5 m/s. The plots also include the backscatters measured by NUSCAT during the Surface Wave Dynamics Experiment (SWADE) in 1991 [42]. As shown,  $\sigma_{hh}$  and  $\sigma_{vv}$  are symmetric functions of  $\phi$ . To study the symmetry properties of the other

polarimetric backscattering coefficients, also included in Figure 4 are the theoretical polarimetric backscattering coefficients. Figures 4(d) and (e) reveal a  $180^\circ$  phase change in  $\rho_{hhhv}$  and  $\rho_{hvvv}$  at the upwind ( $\phi = 0^\circ$ ) and downwind ( $180^\circ$ ) directions, indicating that theoretical correlations between co- and cross-polarized responses from sea surfaces have an odd symmetry. This anti-symmetric feature could potentially reduce the number of ambiguities for ocean wind direction measurements with polarimetric scatterometers.

## V. SUMMARY

The wind direction signals in the brightness temperatures of sea surfaces are analyzed and examined using a two-scale scattering model. This model accounts for the tilting effects of large-scale waves, the anisotropic wavenumber spectrum of short waves, hydrodynamic modulation characterizing the modulation of short waves by long waves and the excess microwave emission from sea foam. Model simulations are found to agree reasonably well with the experimental data from  $0^\circ$  to  $65^\circ$  incidence angles at 19 and 37 GHz.

Contributions of the Bragg scattering by short waves and geometric tilting effects by long waves are examined. It is found that the Bragg scattering mechanism is the dominant scattering source of the wind direction signals in the two-scale model.

In the two-scale model investigated in this paper, the upwind and downwind asymmetry of brightness temperatures is modeled by the hydrodynamic modulations of short waves by long waves. Although the wind speed dependence of the first harmonic coefficients of the Stokes parameters seems to agree with the experimental data, several improvements to the theoretical modeling of polarimetric sea surface brightness temperatures appear necessary. The most likely model components for improvement include the hydrodynamic modulation model of wind-wave interactions and the brightness temperature model of sea foam. It is likely that the hydrodynamic model described by Eq. (14) is too simplistic for sea surfaces and that the spatial distribution of short waves on the faces of long waves may also be a function of wind speed. The second component for improvement is the sea foam emission model. The empirical emission model by Stogryn [37] did not characterize the potential dependence of sea foam properties on the slope of long waves indicated by the data from [38]. However, there are not yet any reliable physical models or experimental data sets, allowing a quantitative determination of sea foam brightness temperatures as a function of surface slopes. Third, the present model does not consider the scattering by breaking waves. Although the areal coverage of breaking waves, like that of sea foam, is usually small, the strong scattering properties of breaking waves have been known to be significant for the microwave backscattering at high incidence angles [22, 41]. Finally, the effects of multiple scattering on the microwave emission from sea surfaces need to be studied, in particular at high incidence angles.

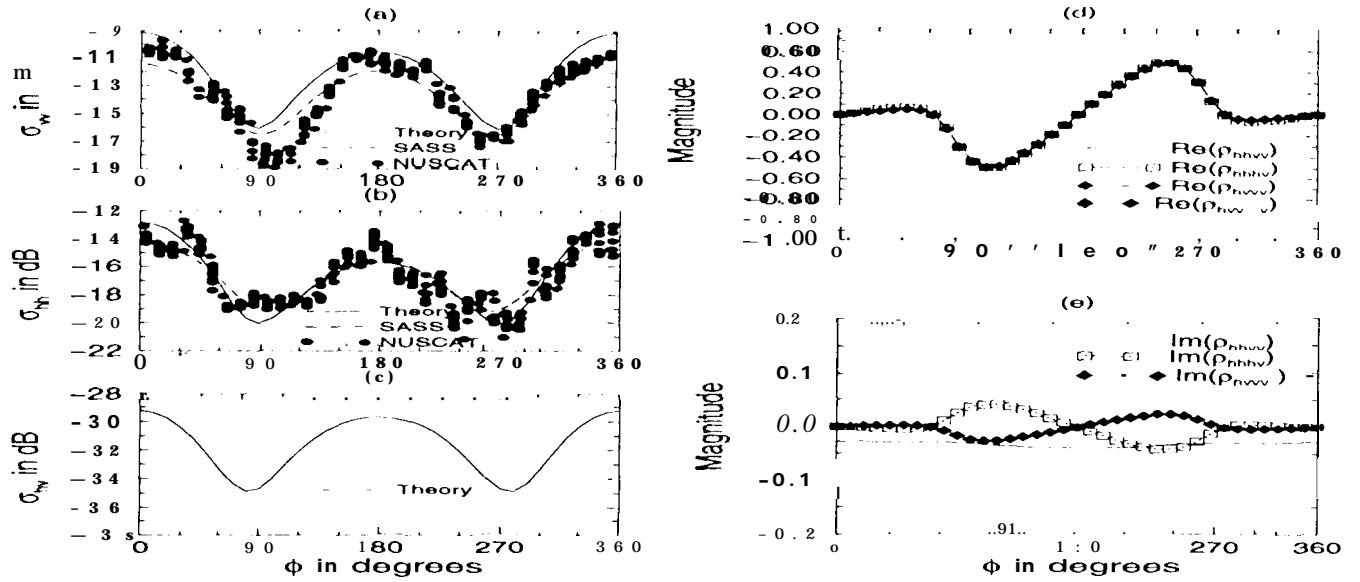


Figure 4. Sea surface backscattering coefficients versus azimuth angle for the wind speed of 11.5 m/s at the incidence angle  $\theta_i = 40^\circ$ : (a)  $\sigma_{vv}$ , (b)  $\sigma_{hh}$ , (c)  $\sigma_{hv}$ , (d) Real parts of correlation coefficients  $\rho_{hhvv}$ ,  $\rho_{hhhv}$ , and  $\rho_{hvvv}$ ; (e) Imaginary parts of correlation coefficients  $\rho_{hhvv}$ ,  $\rho_{hhhv}$ , and  $\rho_{hvvv}$ ; The co-polarized responses  $\sigma_{hh}$  and  $\sigma_{vv}$  include the data calculated from the SASS geophysical model function [7], the data collected by NUSCAT during S WADE [7], and the theoretical sea surface scattering model. The Correlation Coefficients are defined as:  $\rho_{hhvv} = \sigma_{hhv} / \sqrt{\sigma_{hh}\sigma_{vv}}$ ,  $\rho_{hhhv} = \sigma_{hhv} / \sqrt{\sigma_{hh}\sigma_{hv}}$ , and  $\rho_{hvvv} = \sigma_{hvv} / \sqrt{\sigma_{hv}\sigma_{vv}}$ .  $a_0 = 0.008$  and  $k_d = 80 \text{ rad m}^{-1}$ .

## VI. ACKNOWLEDGMENT

The research described in this paper was carried out by the Jet Propulsion Laboratory, California Institute of Technology, under a contract with the National Aeronautics and Space Administration.

### A LOCAL COORDINATE SYSTEM AND VECTOR TRANSFORMATIONS

Given the  $x$  and  $y$  slopes of a tilted flat surface,  $S_x$  and  $S_y$ , the surface normal can be written as:

$$\hat{z}_l = \frac{-S_x \hat{x} - S_y \hat{y} + \hat{z}}{m} \quad (27)$$

However, the surface normal can also be expressed in terms of the zenith and azimuth angles,  $\theta_n$  and  $\phi_n$ , by

$$\hat{z}_l = \sin \theta_n \cos \phi_n \hat{x} + \sin \theta_n \sin \phi_n \hat{y} + \cos \theta_n \hat{z} \quad (28)$$

Equating the above equations allows us to determine  $\theta_n$  and  $\phi_n$ .

Besides the surface normal  $\hat{z}_l$  of the tilted surface, the local  $x$  and  $y$  unit vectors, denoted by  $\hat{x}_l$  and  $\hat{y}_l$ , need to be defined. Because this paper assumes that positive  $x$  is in the wind direction, the  $\hat{x}_l$  vector is chosen to be on the  $x-z$  plane so that the center direction of wind-induced capillary waves on the tilted surface can be conveniently represented by  $\hat{x}_l$ .

$$\hat{x}_l = \cos \beta \hat{x} - \sin \beta \hat{z} \quad (29)$$

$$\hat{y}_l = \hat{z}_l \times \hat{x}_l \quad (30)$$

The angle  $\beta$  is determined by enforcing  $\hat{x}_l$  to be perpendicular to  $\hat{z}_l$ , resulting in

$$\beta = \arctan(\tan \theta_n \cos \phi_n) \quad (31)$$

Carrying out the cross product and using the solution of  $\beta$  give the explicit expression of  $\hat{y}_l$

$$\hat{y}_l = -\sin \theta_n \sin \phi_n (\sin \beta \hat{x} + \cos \beta \hat{z}) + \hat{y} \sqrt{1 - \sin^2 \theta_n \sin^2 \phi_n} \quad (32)$$

Note that as  $\theta_n$  continuously approaches zero, the  $x_l y_l z_l$  coordinate system approaches the global  $x y z$  coordinate system. Additionally, since  $\theta_n$  is expected to be small for sea surfaces,  $\hat{x}_l$  and  $\hat{y}_l$  differ from  $\hat{x}$  and  $\hat{y}$ , respectively, by a small quantity of the order of  $\theta_n^2$ .

By using the above equations, a matrix  $A$  can be defined to recast these vector relations into a matrix form

$$\begin{bmatrix} \hat{x}_l \\ \hat{y}_l \\ \hat{z}_l \end{bmatrix} = A \begin{bmatrix} \hat{x} \\ \hat{y} \\ \hat{z} \end{bmatrix} \quad (33)$$

Here  $A$  is a three-by-three matrix

Hence, the wave vector  $\bar{k}$  expressed in the local coordinate is

$$\bar{k}_l = A \bar{k} \quad (34)$$

From  $\bar{k}_l$ , the local incidence angle  $\theta_l$  and the local azimuth angle  $\phi_l$  can be calculated by the following relation

$$\bar{k}_l = \sin \theta_l \cos \phi_l \hat{x}_l + \sin \theta_l \sin \phi_l \hat{y}_l + \cos \theta_l \hat{z}_l \quad (35)$$

Additionally, the horizontal and vertical polarization vectors,  $\hat{h}_l$  and  $\hat{v}_l$ , can be defined in the local coordinate in

terms of  $\bar{k}_l$  and  $\hat{z}_l$

$$\hat{h}_l = \frac{\bar{k}_l \times \hat{z}_l}{|\bar{k}_l \times \hat{z}_l|} \quad (36)$$

$$\hat{v}_l = \frac{\hat{h}_l \times \bar{k}_l}{|\hat{h}_l \times \bar{k}_l|} \quad (37)$$

Denoting the angle between  $\hat{h}$  and  $\hat{h}_l$  by  $\alpha$  results in

$$\cos \alpha = \hat{v} \cdot \hat{v}_l = \hat{h} \cdot \hat{h}_l \quad (38)$$

$$\sin \alpha = \hat{v} \cdot \hat{h}_l = -\hat{h} \cdot \hat{v}_l \quad (39)$$

The linearly polarized components of electric fields ( $E_v, E_h$ ) in the global coordinate are related to those ( $E_{vl}, E_{hl}$ ) in the local coordinate by

$$E_v = E_{vl} \cos \alpha + E_{hl} \sin \alpha \quad (40)$$

$$E_h = -E_{vl} \sin \alpha + E_{hl} \cos \alpha \quad (41)$$

Hence, it is straightforward to show that the Stokes parameters measured in the global coordinate are related to those measured in the local coordinate by

$$T_v = T_{vl} \cos^2 \alpha + T_{hl} \sin^2 \alpha - U_l \sin \alpha \cos \alpha \quad (42)$$

$$T_h = T_{vl} \sin^2 \alpha + T_{hl} \cos^2 \alpha + U_l \sin \alpha \cos \alpha \quad (43)$$

$$U = U_l (\cos^2 \alpha - \sin^2 \alpha) - (T_{vl} - T_{hl}) \sin 2\alpha \quad (44)$$

$$V = V_l \quad (45)$$

Subscript  $l$  indicates the quantities in the local coordinate.

## B EMPIRICAL SEA SURFACE SPECTRUM

The surface spectrum for a fully developed ocean proposed by Durden and Vesecky [20] has the following form

$$W(k, \phi) = \frac{1}{2\pi k} S(k) \Phi(k, \phi) \quad (46)$$

where the portion of  $S(k)$  with  $k > k_j = 2$  was assumed by Durden and Vesecky based on the dimensional analysis:

$$S(k) = a_0 k^{-3} \left( \frac{b k u_*^2}{g} \right)^{a \log_{10}(k/k_j)} \quad (47)$$

with  $g = g + \gamma k^2$ ,  $\gamma = 7.25 \times 10^{-5}$ , and  $g = 9.81$ . Another three parameters for  $S(k)$  are  $a$ ,  $b$ , and  $a_0$ . The roll-off rate is controlled by  $a$  and  $b$ , and  $a_0$  represents the absolute magnitude of the spectrum. The values of  $a$ ,  $b$ , and  $a_0$  are chosen to be 0.225, 1.25, and 0.008 to best fit the data.

For  $k < k_j = 2$ ,  $S(k)$  is described by the Pierson-Moskowitz spectrum

$$S(k) = b_0 k^{-3} \exp \left[ -0.74 (k_c/k)^2 \right] \quad (48)$$

with  $k_c = g/U_{19.5}^2$ .  $b_0$  is selected in such a way that  $S(k)$  is continuous at  $k = k_j$  for a given  $a_0$ .

The wind speed given at any elevation  $z$  can be calculated from the friction velocity  $u_*$  by

$$U(z) = \frac{u_*}{0.4} \log \left( \frac{z}{Z_0} \right) \quad (49)$$

where  $u_*$  is related to  $Z_0$  by

$$Z_0 = 0.0000684/u_* + 0.00428u_*^2 - 0.000443 \quad (50)$$

The angular portion of the spectrum is assumed to have the following form

$$\Phi(k, \phi) = 1 + c(1 - e^{-sk^2}) \cos 2\phi \quad (51)$$

The coefficients of the angular part of the spectrum are  $s = 1.5 \times 10^{-4}$  and

$$c = \left( \frac{1-RR}{1+R} \right) \frac{2}{(1-D)} \quad (52)$$

where

$$R = \frac{0.003 + 0.00192 U(12.5)}{0.00316 U(12.5)} \quad (53)$$

$$D = \frac{\int_0^\infty k^2 S(k) e^{-sk^2} dk}{\int_0^\infty k^2 S(k) dk} \quad (54)$$

There were misprints in the equations for  $c$ , and  $R$  in [20].

## REFERENCES

- [1] J. P. Hollinger, "Passive microwave measurements of sea surface roughness," *IEEE Trans. Geosci. Electronics*, Vol. GE-9, No. 3, 165-169, July 1971.
- [2] Sasaki, Yasunori, Ichio Asanuma, Kei Muneyama, Gen'ichi Naito, and Tsutomu Suzuki, "The dependence of sea-surface microwave emission on wind speed, frequency, incidence angle, and polarization over the frequency range from 1 to 40 GHz," *IEEE Trans. Geosci. and Remote Sensing*, Vol. GE-25, No. 2, 138-146, March, 1987.
- [3] S. T. Wu and A. K. Fung, "A noncoherent model for microwave emissions and backscattering from the sea surface," *J. Geophys. Res.*, Vol. 77, No. 30, 5917-5929, 1972.
- [4] F. J. Wentz, "A two-scale scattering model for foam-free sea microwave brightness temperatures," *J. Geophys. Res.*, Vol. 80, No. 24, 3441-3446, 1975.
- [5] V. S. Etkin, M. D. Raw, M. G. Bulatov, Yu. A. Militsky, A. V. Smirnov, V. Yu. Raizer, Yu. A. Trokhimovsky, V. G. Irisov, A. V. Kuzmin, K. Ts. Litovchenko, E. A. Bespalova, E. I. Skvortsov, M. h'. Pospelov, and A. I. Smirnov, *Radiohydrophysical Aerospace Research of Ocean*, Report 11P-1749, Academy of Sciences, USSR, Space Research Institute, Moscow, 1991.
- [6] M. S. Dzura, V. S. Etkin, A. S. Khrupin, M. N. Pospelov, and M. D. Raev, "Radiometers-Polarimeters: principles of design and applications for sea surface microwave emission polarimetry," *IEEE, Proceedings of International Geoscience and Remote Sensing Symposium*, Houston, 1992.

- [7] Frank J. Wentz, "Measurement of oceanic wind vector using satellite microwave radiometers," *IEEE Trans. Geosci. Remote Sensing*, Vol. 30, No. 5, 960-972, Sep., 1992.
- [8] S. H. Yueh, W. J. Wilson, F. K. Li, W. B. Ricketts, and S. V. Nghiem, "Polarimetric measurements of sea surface brightness temperatures using an aircraft K-band radiometer," *IEEE Trans. Geosci. Remote Sensing*, Vol. 33, No. 1, 85-92, 1995.
- [9] S. H. Yueh, W. J. Wilson, F. K. Li, S. V. Nghiem, and W. B. Ricketts, "Polarimetric brightness temperatures of sea surfaces measured with aircraft K- and Ka-band radiometers," accepted for publication in *IEEE Trans. Geosci. Remote Sensing*, 1996.
- [10] A. Stogryn, "The Apparent Temperature of the Sea at Microwave Frequencies," *IEEE Trans. Ant. Prop.*, Vol. AP-15, No. 2, 278-286, 1967.
- [11] A. J. Gasiewski, and D. Kunkke, "Polarized microwave emission from water-waves," *Radio Science*, Vol. 29, No. 6, 1449-1466, November-December, 1994.
- [12] C. S. Cox and W. H. Munk, "Measurement of the roughness of the sea surface from photograph's of the sun's glitter," *J. Opt. Soc. Am.*, Vol. 44, 838-850, 1954.
- [13] B. I. Sernyonov, "Approximate computation of scattering of electromagnetic waves by rough surface contours," *Radio Eng. Electron Phys.*, 11, 1179-1187, 1966.
- [14] W. J. Pierson and R. A. Stacy, "The elevation, slope, and curvature spectra of a wind roughened sea surface," Contract Rep. NASA CR-2247, Langley Res. Center, NASA, Harupton, Vs., Dec. 1973.
- [15] L. Tsang, "Polarimetric passive remote sensing of random discrete scatterers and rough surfaces," *J. Electromagnetic Waves and Appl.*, Vol. 5, No. 1, 41-57, 1991.
- [16] S. H. Yueh, R. Kwok, F. K. Li, S. V. Nghiem, W. J. Wilson, and J. A. Kong, "Polarimetric passive remote sensing of ocean wind vector," *Radio Science*, 799-814, July-August, 1994.
- [17] V. G. Irisov, A. V. Kuzmin, M. N. Pospelov, J. G. Trokhimovsky, and V. S. Etkin, "The dependence of sea brightness temperature on surface wind direction and speed. Theory and Experiment.," *IEEE, Proceedings of International Geoscience and Remote Sensing Symposium*, Houston, 1992.
- [18] S. H. Yueh, R. Kwok, F. K. Li, S. V. Nghiem, W. J. Wilson, and J. A. Kong, "Polarimetric passive remote sensing of wind-generated sea surfaces and ocean wind vectors," *Proceedings of Ocean symposium*, Vol. 1, 31-36, Victoria, British Columbia, Canada, October 1993.
- [19] S. H. Yueh, S. V. Nghiem, and R. Kwok, "Comparison of a polarimetric scattering and emission model with ocean backscatter and brightness temperatures," *IEEE, Proceedings of International Geoscience and Remote Sensing symposium*, Pasadena, 1994.
- [20] S. P. Durden and J. F. Vesecky, "A physical radar cross-section model for a wind-driven sea with swell," *IEEE J. Oceanic Eng.*, Vol. C13-10, h'o. 4, 445-451, 1985.
- [21] Allan M. Reece, "h' modulation of short waves by long waves" *Boundary Layer Meteorology*, Vol. 13, 203-214, 1978.
- [22] M. A. Donelan and W. J. Pierson, "Radar scattering and equilibrium ranges in wind-generated waves with applications to scatterometry," *J. Geophys. Res.*, Vol. 92, No. c5, 4971-5029, May 15, 1987.
- [23] W. L. Jones, F. J. Wentz, and L. C. Schroeder, "Algorithm for inferring wind stress from Seasat-A," *J. Spacecr. Rockets*, Vol. 15, 368-374, 1978.
- [24] F. K. Li, G. Neumann, S. Shaffer, and S. L. Durden, "Studies of the location of azimuth modulation minimum for Ku band ocean radar backscatter," *J. Geophys. Res.*, Vol. 93, No. C7, 8229-8238, 1988.
- [25] S. H. Yueh and R. Kwok, "Electromagnetic fluctuations for anisotropic media and the generalized Kirchoff's law," *Radio Science*, Volume 28, No. 4, pp. 471-480, July-August 1993.
- [26] M. E. Veysoglu, S. H. Yueh, R. T. Shin, and J. A. Kong, "Polarimetric passive remote sensing of periodic surfaces," *J. Electromagnetic Waves and Appl.*, Vol. 5, No. 3, 267-280, 1991.
- [27] S. V. Nghiem, M. E. Veysoglu, R. T. Shin, J. A. Kong, K. O'Neill, and A. Lohanick, "Polarimetric passive remote sensing of a periodic soil surface: microwave measurements and analysis" *J. Electromagnetic Waves and Appl.*, Vol. 5, No. 9, 997-1005, 1991.
- [28] S. H. Yueh, S. V. Nghiem, R. Kwok, W. J. Wilson, F. K. Li, J. T. Johnson, and J. A. Kong, "Polarimetric thermal emission from periodic water surfaces," *Radio Science*, Vol. 29, No. 1, 87-96, January-February, 1994.
- [29] J. T. Johnson, J. A. Kong, R. T. Shin, D. H. Staelin, K. O'Neill and A. W. Lohanick, "Third Stokes parameter emission from a periodic water surface," *IEEE Trans. Geosci. Remote Sensing*, Vol. 31, No. 5, 1066-1080, September 1993.
- [30] J. T. Johnson, J. A. Kong, R. T. Shin, S. H. Yueh, S. V. Nghiem, and R. Kwok, "Polarimetric thermal emission from rough ocean surfaces," *J. Electromagnetic Waves and Appl.*, Vol. 8, No. 1, 43-59, 1994.
- [31] S. H. Yueh, R. Kwok, and S. V. Nghiem, "Polarimetric scattering and emission properties of targets with reflection symmetry," *Radio Science*, Vol. 29, h'o. 6, 1409-1420, November-December, 1994.
- [32] John R. Apel, "An improved model of the ocean surface-wave vector spectrum and its effects on radar backscatter," *J. of Geophys. Res.*, Vol. 99, No. c8, 16269-16291, August 1994.
- [33] E. Monahan and I. G. O'Muircheartaigh, *Int. J. Remote Sensing*, Vol. 7, No. 5, 627-642, 1986
- [34] H. I. Chau and A. K. Fung, "A theory for sea scatter at large incidence angles," *J. Geophys. Res.*, Vol. 82, No. 3439-3444, 1977.
- [35] A. K. Fung, and K. K. Lee, "A semi-empirical sea-spectrum model for scattering coefficient estimation," *IEEE J. Oceanic Eng.*, Vol. OE-7, No. 4, 166-176, 1982.
- [36] W. H. Peake, "Interaction of electromagnetic waves with some natural surf aces," *IEEE Trans. Ant. and Prop.* Vol. AP-7, spec. suppl. 8324-8329, 1959
- [37] A. Stogryn, "The Emissivity of Sea Foam at Microwave Frequencies," *J. of Geophys. Res.*, Vol. 77, No. 9, 1658-1666, 1972

- [38] J. M. Smith, "The emissivity of sea foam at 19 and 37 GHz," *IEEE Trans. Geosci. and Remote Sensing*, Vol. GE-26, 541-547, 1988.
- [39] L. A. Klein and C. T. Swift, "An improved model for the dielectric constant of sea water at microwave frequencies," *IEEE Trans. Ant. and Prop.* Vol. AP-25, 104-111, 1977.
- [40] Frank J. Wentz, "A model function for ocean microwave brightness temperatures," *J. Geophys. Res.*, Vol. 88, No. C3, 1892-1908, 1983.
- [41] A. V. Ssrirnov and V. U. Zavorotny, "Study of polarization differences in Ku-band ocean radar imagery," *J. Phys. Oceanography*, Vol. 25, 2215-2228, October 1995.
- [42] Nghiem, S. V., F. K. Li, S. H. Lou and G. Neumann, "Ocean remote sensing with airborne Ku-band scatterometer," *Proceedings of Ocean Symposium*, Vol. 1, 20-24, Victoria, British Columbia, Canada, October 1993.
- [43] Nghiem, S. V., S. H. Yueh, R. Kwok, and N. T. Nguyen, "Polarimetric remote-sensing of geophysical medium structures," *Radio Science*, v28 (6), 1111-1130, Nov-Dec 1993.
- [44] S. H. Yueh, "Modelling of Directional Signals in Polarimetric Sea Surface Brightness Temperatures," *IEEE Trans. Geosci. Remote Sensing*, in press, 1997.
- [45] William J. Wilson and S. H. Yueh, "Results from the JPL Wind Radiometer," *Proceedings of POLRAD-96 Workshop*, European Space Agency, Noordwijk, The Netherlands, 29 April 1997.